ECN-M--08-048

Modelling the effect of wind farming on the mesoscale flow

Part 2: Modification of the velocity profile

A.J. Brand

This paper has been presented at the EWEC 2008,
Brussels (March 31st-April 3rd)

AUGUST 2008

Modelling the effect of wind farming on mesoscale flow - Part 2: Modification of the velocity profile

A J Brand

ECN Wind Energy, P.O. Box 1, NL 1755 RG Petten, Netherlands

E: brand@ecn.nl, T: +31 224 56 4775, F: +31 224 56 8214

Abstract
This paper presents a new method for determining the interaction between a wind farm and the prevailing wind for wind energy siting studies plus first insights on the modification of the wind profile as obtained with this method.

It is shown that neutral planetary boundary layer flow with wind farming essentially is steady and two-dimensional; and that the convective forces, the Coriolis forces and the vertical and spanwise gradients of the turbulent momentum fluxes all have the same order of magnitude. A numerical representation in the form of backward differences allows for an implicit solution of the two horizontal velocity components in vertical direction, iterating on the turbulent viscosity, in combination with a marching solution in the horizontal directions. The continuity equation is satisfied by employing the Lagrange multiplier method to the velocity components that satisfy the continuity equation.

Resolved profiles show how most of the wind speed change occurs in the lower part of the boundary layer whereas most of the wind direction change occurs in the upper part, and that the thinner the boundary layer or the larger the surface roughness, the larger the wind direction change. Near a 5 MW wind turbine with a rotor diameter of 100 m operating at full load the velocity deficit is of the order of 5%, the wind direction change is increased with 1 ... 2 deg, and the velocity recovery distance is 20 rotor diameters. For a wind farm with 22 of these turbines these numbers are 15%, 2 ... 3 deg, and 2 wind farm length scales

1. Introduction

Offshore wind farms tend to be placed closer together over the years, as already illustrated by OWEZ and Q7-WF (separated 15 km) in the Netherlands or Horns Rev I and II (separated 23 km) in Denmark. Since these separation distances are between 5 and 10 times the wind farm's horizontal scale, the velocity deficit due to an upstream wind farm may be considerable [1]. If so, energy production loss and mechanical load increase are expected to be significant. For this reason wind farm wake studies have gained attention recently.

In this paper we present a new method for determining the interaction between a wind farm and the prevailing wind, and first insights on the modification of the wind profile as obtained with this method. First, section 2 gives a brief description of prior work on modelling wind farm wakes. Next, section 3 presents the new flow model, and section 4 presents velocity profiles obtained with this flow model. Finally, in section 5 we summarize the new model and the first insights, and introduce the future developments.

2. Prior work

A wind farm wake study requires simulation of mesoscale atmospheric flow together with energy extraction/redistribution due to wind turbines. The studies that have been published so far can be subdivided into two categories: self-similar approaches and mesoscale approaches. In a self-similar approach [2][3] the convective force and the spanwise turbulent flux gradients are assumed to dominate the flow, allowing for standard wake-like solutions. In a mesoscale approach, on the other hand, the flow is assumed to be dominated by the Coriolis force and the vertical turbulent flux gradients, opening the door to either extra surface drag approaches [4] or more generic mesoscale approaches [5][6][7]. As will be shown in section 3.3 of this paper, neither the self-similar wake approach nor the extra surface drag approach is valid because over the separation distance between wind farms the convective and the Coriolis forces are of equal order of magnitude so that neither can be neglected. Although this was already implicitly recog-

nized in the more generic approaches, these studies lack realistic formulations for the turbulence and the wind turbines.

3. Flow model

3.1. Overview

In section 3.2 first we introduce the flow problem. Next, in section 3.3 we derive the governing equations from the planetary boundary layer equations and the continuity equation by employing a scale analysis, modelling Reynolds stresses with turbulent viscosity and wind turbines with body forces. Since these equations are essentially steady and two-dimensional (the vertical wind speed scale is several orders of magnitude smaller than a horizontal wind speed scale), the pressure gradients can be treated as geostrophic wind speed components. Next, in section 3.4 we sketch the derivation of a numerical representation of the non-dimensional momentum equations by using finite differences. The resulting scheme is implicit in vertical direction, iterating between the two horizontal velocity components and the turbulent viscosity, and allows for a marching solution in the horizontal directions. Subsequently, in section 3.5 we address the continuity equation which is not automatically satisfied when the momentum equations are solved. In order to obtain a velocity which does satisfy continuity the Lagrange multiplier method is applied. We then turn attention to the turbulence parameterization in section 3.6, and to the wind turbine parameterization in section 3.7. Finally, we present the boundary conditions and initial conditions in section 3.8.

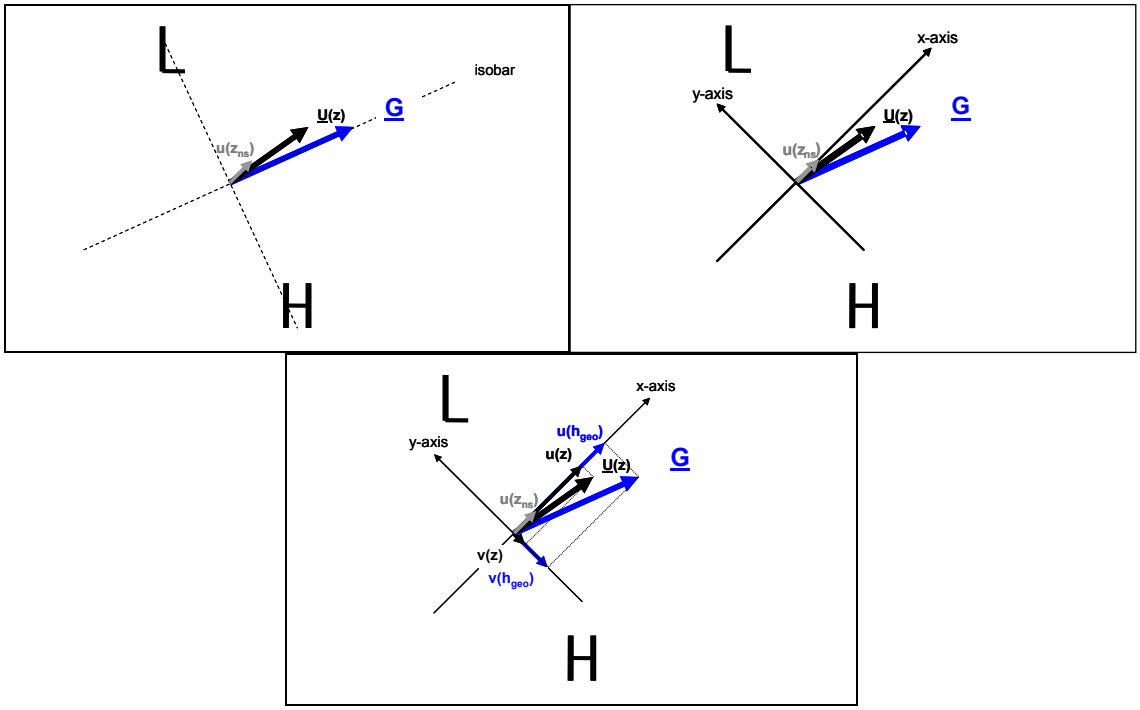

Figure 1. Velocity decomposition. (a) Geostrophic wind G and near-surface wind $u(z_{ns})$. (b) Streamwise axis x in the direction of the near-surface wind. (c) Streamwise component u(z) and spanwise component v(z) of the geostrophic wind

3.2. Flow problem

Consider the geostrophic wind, that is the theoretical wind that results from the balance between the pressure gradient force and the Coriolis force (figure 1a). This wind is directed parallel to lines of equal pressure, with low pressure on the left on the northern hemisphere. Turbulent drag slows the wind and turns it to point towards low pressure. Near the surface the deviation

form geostrophic is largest. Next consider an observer who looks in the direction of the near-surface wind, and introduce the x-axis likewise (figure 1b). Then for the observer the wind points towards the high pressure, which means that in his coordinate system the surface wind has a negative spanwise component. By the way, now the flow problem has been introduced: Determine the velocity components observed at a given height by an observer who looks in the direction of the near surface wind, given a geostrophic wind and a surface roughness. Now replace the passive observer by a wind turbine that exerts a force on the wind, and the flow problem has been defined (figure 1c).

3.3. Governing equations

The mean (in the sense of Reynolds averaged) flow in the neutral planetary boundary layer is incompressible and high-Reynolds number. In addition, as explained in section 3.2, it is turbulent and affected by the rotation of the earth. It is described by the momentum equations [8, section 5.2.1]:

$$\frac{\partial \bar{u}}{\partial t} + \bar{u}\frac{\partial \bar{u}}{\partial x} + \bar{v}\frac{\partial \bar{u}}{\partial y} + \bar{w}\frac{\partial \bar{u}}{\partial z} = -\frac{1}{\rho}\frac{\partial \bar{p}}{\partial x} + f_\phi \bar{v} - \frac{\partial \overline{u'u'}}{\partial x} - \frac{\partial \overline{u'v'}}{\partial y} - \frac{\partial \overline{u'w'}}{\partial z} + \bar{a}_x \tag{1}$$

$$\frac{\partial \bar{v}}{\partial t} + \bar{u}\frac{\partial \bar{v}}{\partial x} + \bar{v}\frac{\partial \bar{v}}{\partial y} + \bar{w}\frac{\partial \bar{v}}{\partial z} = -\frac{1}{\rho}\frac{\partial \bar{p}}{\partial y} - f_\phi \bar{u} - \frac{\partial \overline{v'u'}}{\partial x} - \frac{\partial \overline{v'v'}}{\partial y} - \frac{\partial \overline{v'w'}}{\partial z} + \bar{a}_y \tag{2}$$

$$\frac{\partial \bar{w}}{\partial t} + \bar{u}\frac{\partial \bar{w}}{\partial x} + \bar{v}\frac{\partial \bar{w}}{\partial y} + \bar{w}\frac{\partial \bar{w}}{\partial z} = -\frac{1}{\rho}\frac{\partial \bar{p}}{\partial z} - \frac{\partial \overline{w'u'}}{\partial x} - \frac{\partial \overline{w'v'}}{\partial y} - \frac{\partial \overline{w'w'}}{\partial z} + \bar{a}_z \tag{3}$$

in combination with the continuity equation:

$$\frac{\partial \bar{u}}{\partial x} + \frac{\partial \bar{v}}{\partial y} + \frac{\partial \bar{w}}{\partial z} = 0\,; \tag{4}$$

and a set of boundary conditions. Here

- $\bar{u}$, $\bar{v}$ and $\bar{w}$ are the components of the mean velocity;
- u', v' and w' are the velocity fluctuations;
- ρ is the air density;
- $\bar{p}$ is the mean pressure;
- f_ϕ is the Coriolis parameter;
- $\bar{a}_x$, $\bar{a}_y$ and $\bar{a}_z$ are the mean components of the flow acceleration due to the external body force in this case exerted by wind turbines; and
- the covariances represent the turbulent momentum fluxes.

The z-axis is in vertical direction and without loss of generality the x-axis is assumed to be in the direction of the surface wind. The equations (1), (2), (3) and (4) constitute a system of 4 equations with 4 unkowns, which can be solved once boundary conditions are set. We come back to the boundary conditions in section 3.8.

The magnitude of the individual terms in the equations (1), (2), (3) and (4) are estimated by performing a scale analysis [9, section 3.2]. By neglecting the small terms, it follows that also in the case of wind farming the neutral planetary boundary layer equations are essentially steady and two-dimensional:

$$\bar{u}\frac{\partial \bar{u}}{\partial x} + \bar{v}\frac{\partial \bar{u}}{\partial y} = +f_\phi\left(\bar{v} - v_g\right) - \frac{\partial \overline{u'v'}}{\partial y} - \frac{\partial \overline{u'w'}}{\partial z} + \bar{a}_x \tag{5}$$

$$\bar{u}\frac{\partial \bar{v}}{\partial x} + \bar{v}\frac{\partial \bar{v}}{\partial y} = -f_\phi\left(\bar{u} - u_g\right) - \frac{\partial \overline{v'v'}}{\partial y} - \frac{\partial \overline{v'w'}}{\partial z} + \bar{a}_y \tag{6}$$

$$\frac{\partial \bar{u}}{\partial x} + \frac{\partial \bar{v}}{\partial y} = 0\,, \tag{7}$$

where u_g and v_g by definition are the components of the geostrophic velocity reached far from the surface. But in contrast to standard geostrophic flow the convective force and the y-wise turbulent momentum flux gradients are maintained, which rules out extra surface drag ap-

proaches. Also note that in contrast to general wake flow the Coriolis force and the vertical turbulent momentum flux gradients are maintained, ruling out self-similar wake approaches.

In contrast to the original system the equations (5), (6) and (7) constitute an overdetermined system: 3 equations with 2 unknowns. Since evidently the velocity must obey conservation of mass, the solution to the momentum equations must be corrected in such a way that the velocity satisfies continuity while remaining close to that solution. This is achieved by using the Lagrange multiplier method [10, section 7.7], which essentially provides the third unknown. We come back to this in section 3.5.

Another scale analysis, the Rossby-number similarity approach [11, section 3.2.1], shows that close to the surface the x-wise velocity component of geostrophic flow is much larger than the y-wise velocity component. At first approximation the near-surface wind is therefore in the x-direction. For this reason in the following the x-direction is referred to as the streamwise direction, and the y-direction as the spanwise direction.

In order to close the momentum equations (5) and (6) the turbulent momentum fluxes are re presented by a mean turbulent viscosity $\overline{k_m}$ in combination with gradients of the mean velocity components:

$$\overline{u'v'} = -\overline{k_m}\left(\frac{\partial \bar{u}}{\partial y} + \frac{\partial \bar{v}}{\partial x}\right), \quad \overline{u'w'} \approx -\overline{k_m}\frac{\partial \bar{u}}{\partial z}, \quad \overline{v'v'} \approx -2\overline{k_m}\frac{\partial \bar{u}}{\partial y} \quad \text{and} \quad \overline{v'w'} \approx -\overline{k_m}\frac{\partial \bar{v}}{\partial z}. \tag{8}$$

The approximations here originate from a scale analysis of the turbulent fluxes [9, section 3.2]. Note the equations are not closed completely because the mean turbulent viscosity remains; its parameterization is addressed in section 3.6.

The external accelerations in the momentum equations (5) and (6) require another form of closure because these accelerations, due to the force exerted by the wind turbines, ultimately depend on the horizontal velocity. We treat this in section 3.7.

By inserting the expressions (8) for the turbulent momentum fluxes into the momentum equations (5) and (6), and by applying the continuity equation (7), we obtain:

$$-\bar{u}\frac{\partial \bar{v}}{\partial y} + \bar{v}\frac{\partial \bar{u}}{\partial y} = f_\phi\left(\bar{v} - v_g\right) + \frac{\partial \overline{k_m}}{\partial y}\left(\frac{\partial \bar{u}}{\partial y} + \frac{\partial \bar{v}}{\partial x}\right) + \overline{k_m}\left(\frac{\partial^2 \bar{u}}{\partial y^2} + \frac{\partial^2 \bar{v}}{\partial y \partial x} + \frac{\partial^2 \bar{u}}{\partial z^2}\right) + \frac{\partial \overline{k_m}}{\partial z}\frac{\partial \bar{u}}{\partial z} + \overline{a_x} \tag{9}$$

$$\bar{u}\frac{\partial \bar{v}}{\partial x} - \bar{v}\frac{\partial \bar{u}}{\partial x} = -f_\phi\left(\bar{u} - u_g\right) + 2\frac{\partial \overline{k_m}}{\partial y}\frac{\partial \bar{u}}{\partial y} + \overline{k_m}\left(2\frac{\partial^2 \bar{u}}{\partial y^2} + \frac{\partial^2 \bar{v}}{\partial z^2}\right) + \frac{\partial \overline{k_m}}{\partial z}\frac{\partial \bar{v}}{\partial z} + \overline{a_y} \tag{10}$$

$$\frac{\partial \bar{u}}{\partial x} + \frac{\partial \bar{v}}{\partial y} = 0. \tag{11}$$

The momentum equations (9) and (10), together with the continuity equation (11), are the governing equations for neutral planetary boundary layer flow with wind farming.

3.4. Solution procedure momentum equations

First, the momentum equations (9) and (10) are casted in non-dimensional form, employing linear transformations in the horizontal directions and an exponential transformation in the vertical direction. Next a numerical representation of the non-dimensional momentum equations is derived by using finite differences. (The complete derivation has been published separately [9, sections 3.2.2 and 3.3].) Since the velocity depends on the turbulent viscosity, the resulting solution procedure iterates between solving a relatively small matrix-vector system by Gaussian elimination and computing the turbulent viscosity profile. The procedure starts in the vertical at [i+1,j+2] so that initial velocity conditions are needed at the inlet plane i = 1 and the two planes at j = 1 and j = 2, and initial turbulent viscosity conditions also at [i,j]. Once a vertical profile of U and V is computed in [i,j], the procedure proceeds with the profiles in [i,j+1], [i,j+1] etc. until j_{max} is reached. Next follow the planes at i+1, i+2 etc up to i_{max}. The solution therefore marches in the two horizontal directions.

3.5. To satisfy the continuity equation

A solution to the momentum equations (9) and (10) does not automatically satisfy the continuity equation. In order to derive a velocity that does satisfy continuity we apply the Lagrange multi-

plier method [10, section 7.7]. This method basically provides the third unknown to the system of equations by applying a Poisson solver to the divergence of the velocity field, and subsequently computes the gradient of the so-determined third unknown.

Now consider the components $\bar{u}_m$ and $\bar{v}_m$ of the velocity that satisfies the momentum equations. According to the Lagrange multiplier method the looked-after third unknown λ is given by

$$\frac{\partial^2\lambda}{\partial x^2}+\frac{\partial^2\lambda}{\partial y^2}+\frac{\partial^2\lambda}{\partial z^2}=\frac{\partial\bar{u}_m}{\partial x}+\frac{\partial\bar{v}_m}{\partial y}\,, \tag{12}$$

with Neumann boundary conditions

$$\frac{\partial\lambda}{\partial x}=0 \text{ and } \frac{\partial\lambda}{\partial y}=0$$

at the faces of the computational domain because a correction to the velocity is not needed there. The gradient of the third unknown is equal to the velocity correction, so that

$$\bar{u}_{c+m}=\bar{u}_m-\frac{\partial\lambda}{\partial x} \quad \text{and} \quad \bar{u}_{c+m}=\bar{u}_m-\frac{\partial\lambda}{\partial x}$$

are the components of the velocity that satisfy both momentum and continuity.

3.6. Turbulence parameterisation

The mean turbulent viscosity $\overline{k_m}$ in the momentum equations (9) and (10) is parameterized by using the algebraic Baldwin-Lomax model [12, section 3.4.2] [9, section 3.4].

3.7. Wind turbine parameterization

The external acceleration in the momentum equation is due to the force exerted on the flow by a wind turbine, which force - apart from the sign - is equal to the thrust on the rotor. The rotor thrust essentially depends on the velocity induced by the rotor of a wind turbine, which in turn is related to the power production and thus to the horizontal velocity at hub height. Evidently the external acceleration is only present in a grid point where a wind turbine rotor is located or the grid points where a rotor is interpolated; it is zero in any other grid point [9, section 3.5].

3.8. Initial and boundary conditions

3.8.1. Boundary conditions Mean velocity boundary conditions have already been introduced in section 3.3: zero at the bottom of the numerical domain (corresponding to z_0) and geostrophic at its top (corresponding to h_{geo}). The boundary conditions for the mean turbulent viscosity are included in its parameterization (see section 3.6): vanishing but non-zero at both the bottom and the top of the numerical domain.

3.8.2. Initial conditions Velocity initial conditions are needed in the inlet plane i = 1 and in the planes j = 1 and j = 2. These are inspired by the Rossby-number similar planetary boundary layer velocity profiles [11, section 3.2.1], and comprise a logarithmic profile for the non-dimensional streamwise velocity and a linear profile for the non-dimensional spanwise velocity:

$$U(z)=\left(1-\frac{\ln(z/h_{geo})}{\ln(z_0/h_{geo})}\right)\frac{v_g}{G} \quad \text{and} \quad V(z)=\frac{z-z_0}{h_{geo}-z_0}\frac{v_g}{G} \tag{13}$$

where z is the distance from the surface. The initial profile for the mean turbulent viscosity, also needed in the vertical at [i, j], is obtained by applying the Baldwin-Lomax model to the profiles (13). As an example figure 2 shows the initial profiles for a geostrophic height of 500 m and a surface roughness length of 0.1 mm.

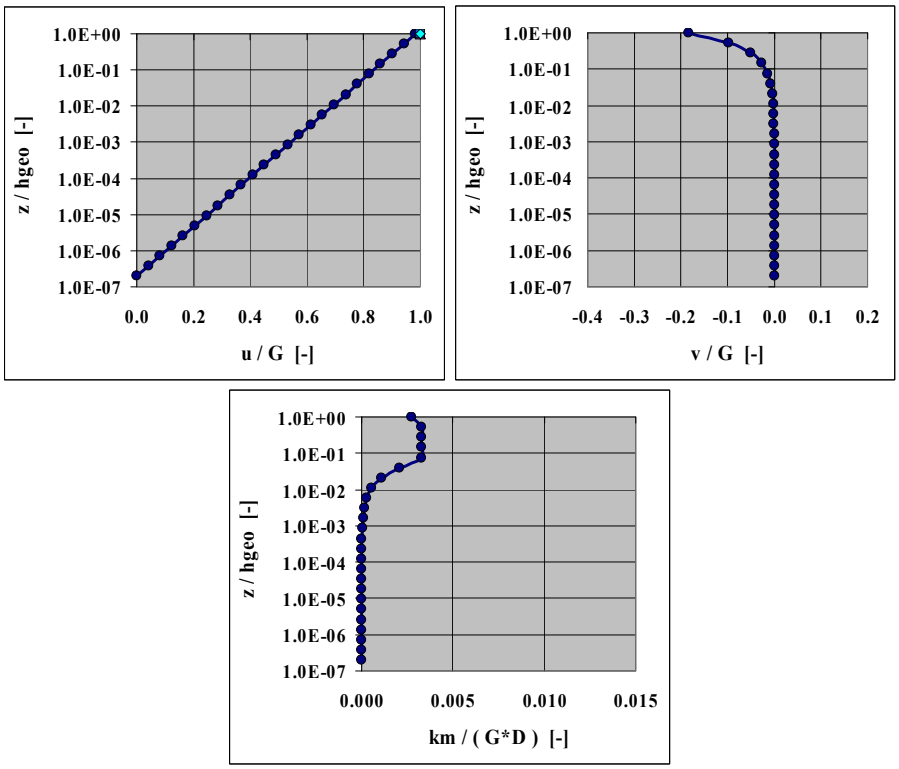

Figure 2. Initial profiles of streamwise velocity u, spanwise velocity v and turbulent viscosity k_m as non-dimensionized with the geostrophic velocity G, the geostrophic height h_{geo} and the rotor diameter D; valid for a geostrophic height of 500 m and a surface roughness length of 0.1 mm

4. Resolved velocity profiles

4.1. Empty set

In this section the resolved velocity profiles for the empty set, that is a domain without wind farming, are presented. Figure 3 shows four vertical profiles in a 200 x 200 km^2 domain, and valid for a geostrophic height of 500 m and a surface roughness length of 0.1 mm. The figures display the streamwise velocity versus height, the spanwise velocity, the angle between the streamwise and the spanwise velocity, and a hodograph of the two velocity components. The data in the figure is in qualitative agreement with the observed height dependence of undisturbed wind, where most of the velocity change occurs in the lower part and most of the direction change occurs in the upper part of the boundary layer, but it is too early to decide on the quantitative agreement.

The figures 4 and 5 display a much thicker boundary layer (1500 m) with the same surface roughness, and the same boundary layer thickness in combination with a much rougher surface (1 cm). The figures show that the thinner the boundary layer or the larger the surface roughness, the larger the twist in the velocity profile. Again this qualitative agreement with observations is to be collaborated with quantitative data.

The data in the figures 2 to 5 was obtained with a horizontal grid size of 2 x 2 km^2. Figure 6 shows that a further refinement has a low impact on the velocity profiles.

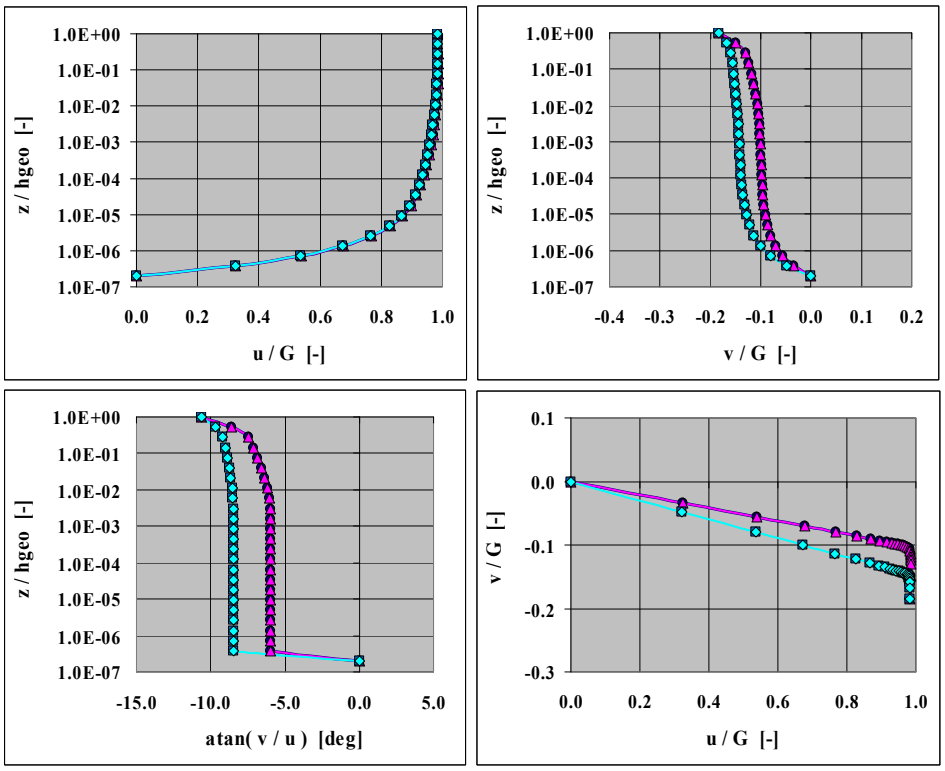

u_g = 16.0 m/s
v_g = –3.0 m/s
h_{geo} = 500 m
z_0 = 0.1 mm
L_x = L_y = 200 km
N_x = N_y = 101
N_z = 25
x = 16 and 32 km
y = 88 and 104 km

Figure 3. Vertical profiles for a geostrophic height of 500 m and a surface roughness length of 0.1 mm; see caption of figure 2 for an explanation of the symbols

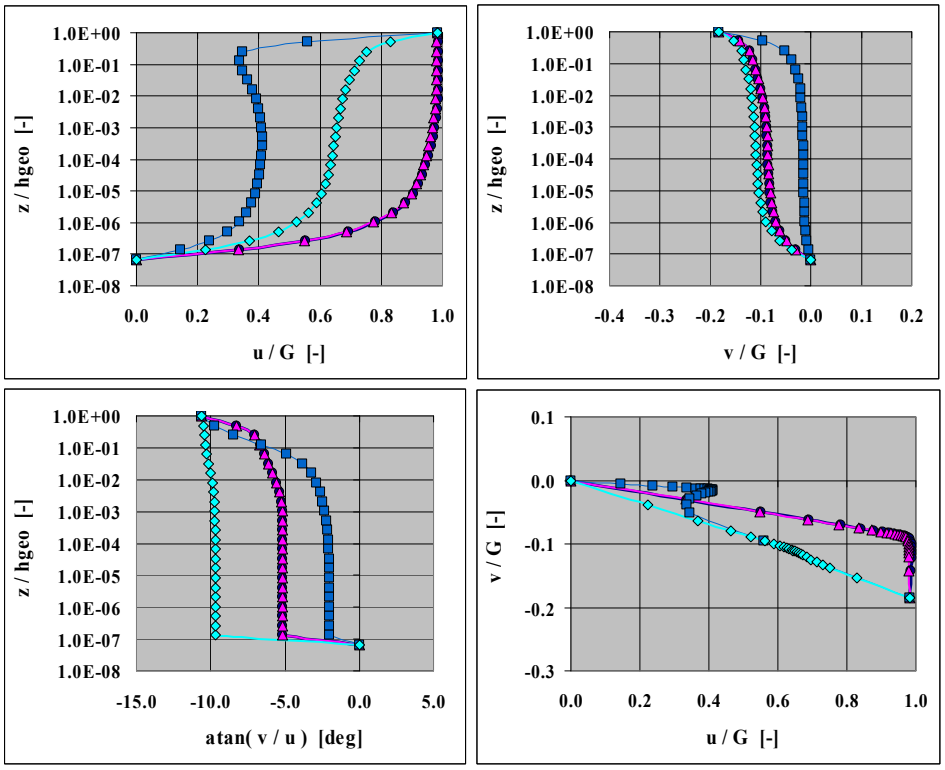

u_g = 16.0 m/s
v_g = –3.0 m/s
h_{geo} = 1500 m
z_0 = 0.1 mm
L_x = L_y = 200 km
N_x = N_y = 101
N_z = 25
x = 16 and 32 km
y = 88 and 104 km

Figure 4. Vertical profiles for a geostrophic height of 1500 m and a surface roughness length of 0.1 mm; see caption of figure 2 for an explanation of the symbols

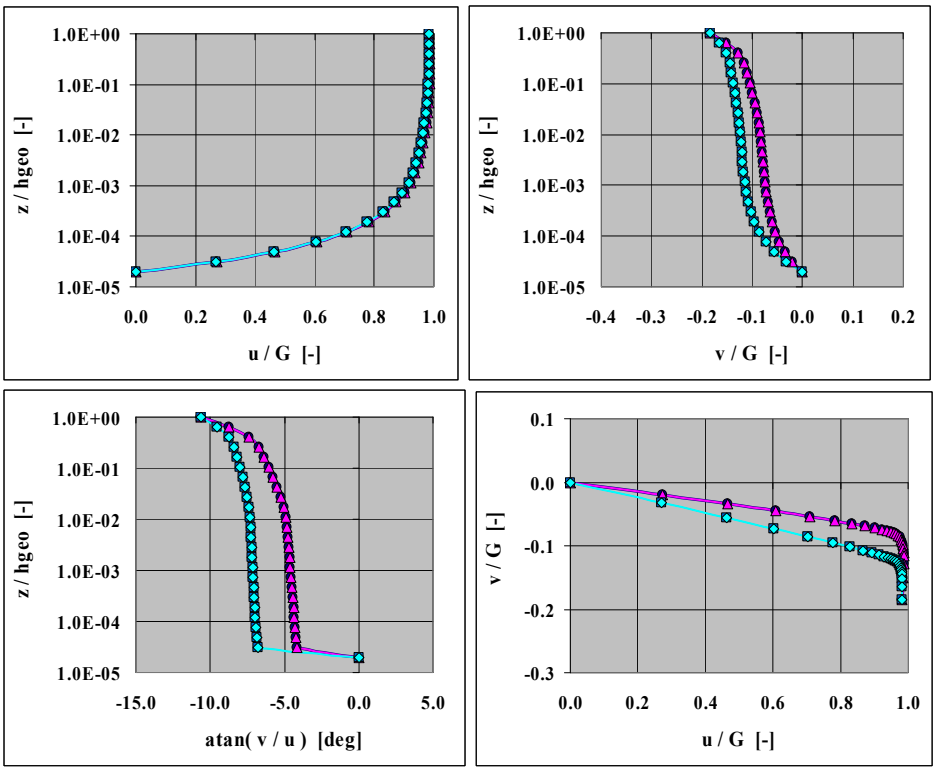

u_g = 16.0 m/s
v_g = −3.0 m/s
h_{geo} = 500 m
z_0 = 10 mm
L_x = L_y = 200 km
N_x = N_y = 101
N_z = 25
x = 16 and 32 km
y = 88 and 104 km

Figure 5. Vertical profiles for a geostrophic height of 500 m and a surface roughness length of 1 cm; see caption of figure 2 for an explanation of the symbols

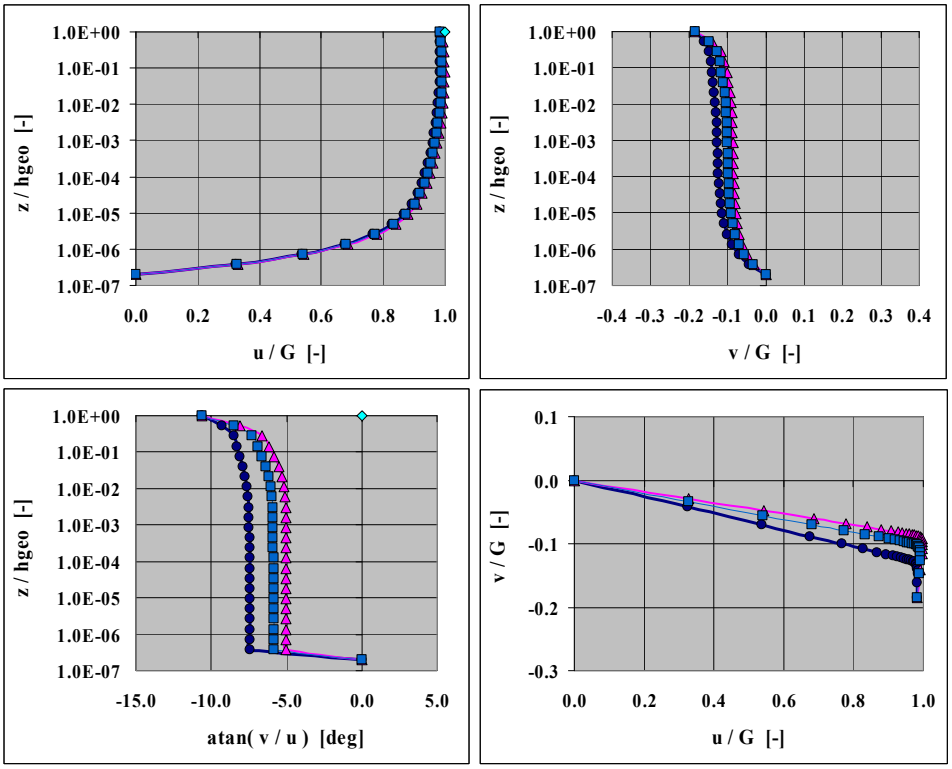

u_g = 16.0 m/s
v_g = −3.0 m/s
h_{geo} = 500 m
z_0 = 0.1 mm
L_x = L_y = 200 km
N_x = N_y =101, 51 and 26
N_z = 25
x = 24 km
y = 96 km

Figure 6. Vertical profiles for a geostrophic height of 500 m and a surface roughness length of 0.1 mm; horizontal grid size 8 km, 4 km and 2 km; see caption of figure 2 for an explanation of the symbols

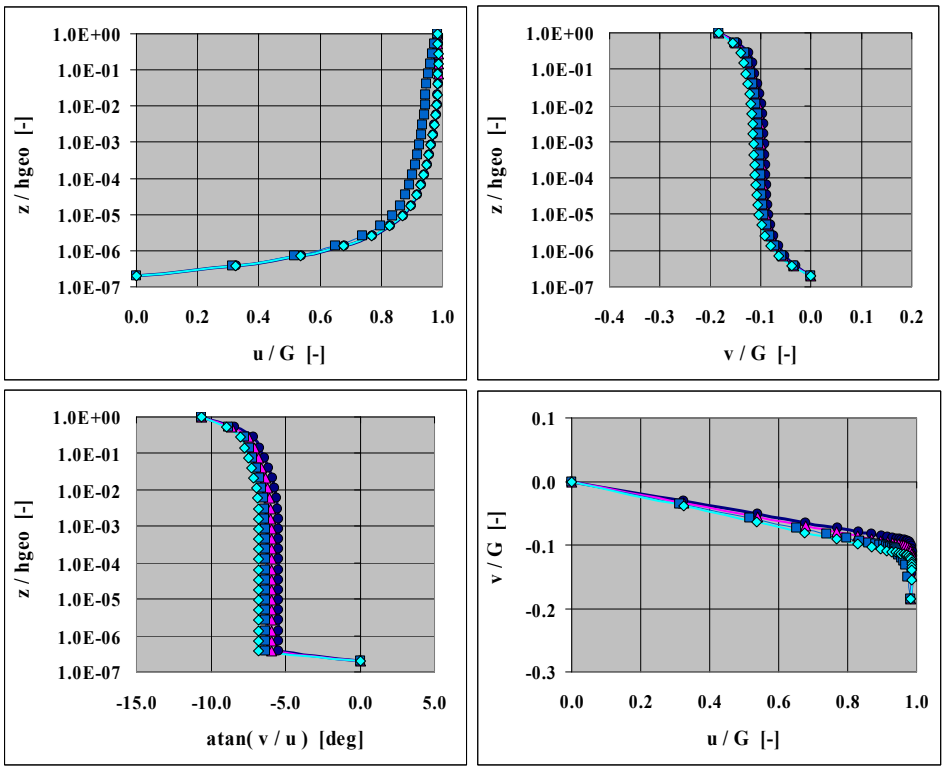

u_g = 16.0 m/s
v_g = –3.0 m/s
h_{geo} = 500 m
z_0 = 0.1 mm
z_{hub} = 70 m
D = 100 m
A_{ffarm} = 1 km^2
$P_{nom,farm}$ = 5 MW
L_x = L_y = 200 km
N_x = N_y = 101
N_z = 25
s_x = –4, –2, 0 and +2 km

Figure 7. Vertical profiles upstream, near and downstream of a wind turbine for a geostrophic height of 500 m and a surface roughness length of 0.1 mm

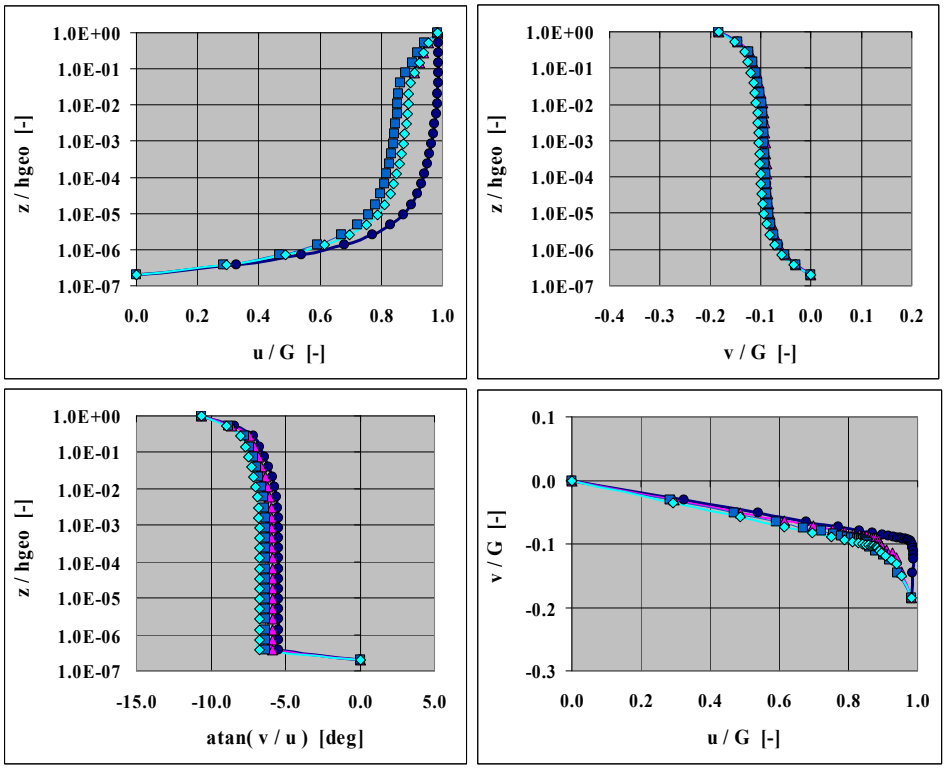

u_g = 16.0 m/s
v_g = –3.0 m/s
h_{geo} = 500 m
z_0 = 0.1 mm
z_{hub} = 70 m
D = 100 m
A_{ffarm} = 22 km^2
$P_{nom,farm}$ = 110 MW
L_x = L_y = 200 km
N_x = N_y = 101
N_z = 25
s_x = –4, –2, 0 and +2 km

Figure 8. Vertical profiles upstream, near and downstream of a wind farm for a geostrophic height of 500 m and a surface roughness length of 0.1 mm

4.2. Wind turbine and wind farm

The modification of the wind profile due to an hypothetical wind turbine is studied for a turbine with a nominal power of 5 MW operating at full load, and having a rotor diameter of 100 m and a hub height of 70 m. Figure 7 shows that the initial velocity deficit is of the order of 5% and that the velocity twist is increased with 1 ... 2 deg. The velocity recovery distance is 20 rotor diameters.

The hypothetical wind farm has a nominal power density of 5 MW/km^2. It consists of 22 turbines with a rotor diameter of 100 m, a hub height of 70 m and a nominal power of 5 MW. Figure 8 shows that if the wind farm operates at full load the initial velocity deficit is of the order of 15% and that the velocity twist is increased with 2 ... 3 deg. The velocity recovery distance is of the order of 2 wind farm length scales.

5. Summary and future

A new method for determining the interaction between a wind farm and the prevailing wind for wind energy siting studies plus first insights on the modification of the wind profile as obtained with this method have been presented.

It has been shown that neutral planetary boundary layer flow with wind farming essentially is steady and two-dimensional; and that the convective forces, the Coriolis forces and the vertical and spanwise gradients of the turbulent momentum fluxes all have the same order of magnitude. In addition it has been shown that a numerical representation in the form of backward differences allows for an implicit solution of the two horizontal velocity components in vertical direction, iterating on the turbulent viscosity, and a marching solution in the horizontal directions. And finally it has been shown how the continuity equation is satisfied by employing the Lagrange multiplier method to the velocity components that satisfy the continuity equation.

Resolved profiles have been presented that show how most of the wind speed change occurs in the lower part of the boundary layer whereas most of the wind direction change occurs in the upper part. The profiles also show that the thinner the boundary layer or the larger the surface roughness, the larger the wind direction change. Also it has been shown that near a wind turbine with a rotor diameter of 100 m operating at a full load of 5 MW the velocity deficit is of the order of 5%, the wind direction change is increased with 1...2 deg, and the velocity recovery distance is 20 rotor diameters. Finally it has been shown that or a wind farm with 22 of these turbines these numbers are 15%, 2...3 deg, and 2 wind farm length scales, respectively.

Subsequently the new method will be further developed and applied. Insights that will be derived will include the impact of separation distance from and layout (spacing, energy density) of the wind farm, the impact of hub height and rotor diameter of the wind turbine, and the impact of geostrophic velocity, geostrophic height and surface roughness.

Acknowledgements

This work was performed in the Dutch Ministry of Economic Affairs BSIK programme We@Sea, project "Windenergiecentrale Noordzee - Parkinteractie" (We@Sea/BSIK 2005/002).

References

[1] Christiansen MB and Hasager CB 2005. 31st Int. Symp on Remote Sensing of Environment, St Petersburg, Russian Federation
[2] Frandsen S et al. 2004. Report Risø-R-1518(EN)
[3] Hegberg T 2004. Report ECN-C--04-033
[4] Hegberg T 2002. Global Wind Power Conference 2002, Paris, France
[5] Liu M-K et al. 1983. J. Energy, Vol. 7, No. 1, pp. 73-78
[6] Baidya Roy S et al. 2004. J. Geoph. Research, Vol. 109, D19101
[7] Rooijmans P 2004. Universiteit Utrecht, Masters thesis
[8] Holton J R 1992. Academic Press
[9] Brand A J 2007. J. of Physics: Conf. Series 75 (2007) 012043
[10] Ferziger JH and Perić M 1997. Springer
[11] Garratt JR 1994. Cambridge University Press
[12] Willcox DC 1998. DCW Industries Inc.